

Todo list

Get a picture of EGRET to include	11
Short description of the history of TeV astronomy	12
What is the LAT effective area?	12
Make note of “Air force had early warning of pulsars” paper	13
First gamma-ray detection	14
When was the PSR, PWN connection made	14
XXXXXXXXXXXXXXXXXXXXXXXXXXXXXXXXXXXXXXXXXXXXXXXXXXXXXXXXXXXXXXXXXXXX	
Get image of Synchrotron radiation (from R&L to include in discussion. . . .	18
Why no Bremsstrahlung radiation from PWN. Maybe a back-of-the-envelope estimate	21
Describe the characteristic π^0 cutoff energy	21
Include discussion of modeling, if time permitting	21
Describe Catalog	22
Dig up HESS reference of HESS J1514-59.	23
Where are sites of acceleratoin	30
Discuss pulsar evolution “The Evolution and Structure of Pulsar Wind Nebulae” – Bryan M. Gaensler and Patrick O. Slane	34
Describe Mattana’s work on pulsar wind nebulae (PWNe): “On the evolution of the Gamma- and X-ray luminosities of Pulsar Wind Nebulae”	34
Describe SNR Reverse Shock	35
Include discussion of cooling in Matanna et al 2009 (equation 12	36
Look up scaling relationships for IC and Sync radiation from Adam Van Etten’s thesis	36

what section discusses energy dependent psf?	38
What are the benefits of maximum likelihood	39
Describe Wilk's Therorem and it's application to parameter error estimation .	39
WHAT SECTION DESCRIBES EXTENDED SOURCE PDFs	41
FINISH DISCUSSION	41
Discuss how diffuse background is more complciated and requires a mapcube.	41
LINK TO arXiv:1206.1896 for MORE THOUROUGH DISCUSSION OF EF- FECTIVE AREA	42
DISCUSS HOW EFFECTIVE AREA IS A FUNCTION OF DIFFERENT THINGS	42
What is the range of the integrals	42
BETTER DISCUSSION OF PSF OF THE LAT, WHAT ITS SCALE IS... .	43
Why discard time dispersion	43
WRITE ENERGY DISPERSION AS A DELTA FUNCTION	43
FINISH	44
Figure out how the θ depedence of the IRFs factors into this calcualtion . . .	44
Write Section or Perform simple MC Simulation to demonstrate significance of detection	45
WHERE ARE RESULTS PRESENTED	128
What would make good future work. Something about CTA population study, something about improved modeling liek HESS J1825, something about better PSF	137

OBSERVATIONS OF PWNE WITH THE FERMI GAMMA-RAY
SPACE TELESCOPE

A DISSERTATION
SUBMITTED TO THE DEPARTMENT OF PHYSICS
AND THE COMMITTEE ON GRADUATE STUDIES
OF STANFORD UNIVERSITY
IN PARTIAL FULFILLMENT OF THE REQUIREMENTS
FOR THE DEGREE OF
DOCTOR OF PHILOSOPHY

Joshua Jeremy Lande

April 2013

© Copyright by Joshua Jeremy Lande 2013
All Rights Reserved

I certify that I have read this dissertation and that, in my opinion, it is fully adequate in scope and quality as a dissertation for the degree of Doctor of Philosophy.

(Stefan Funk) Principal Adviser

I certify that I have read this dissertation and that, in my opinion, it is fully adequate in scope and quality as a dissertation for the degree of Doctor of Philosophy.

(Elliott Bloom)

I certify that I have read this dissertation and that, in my opinion, it is fully adequate in scope and quality as a dissertation for the degree of Doctor of Philosophy.

(Roger Romani)

Approved for the University Committee on Graduate Studies

Contents

Abstract	iv
Acknowledgement	v
1 Overview	3
2 Gamma-ray Astrophysics	4
2.1 Astronomy and the Atmosphere	4
2.2 The History of Gamma-ray Astrophysics	5
2.3 The <i>Fermi</i> Gamma-ray Space Telescope	12
2.3.1 The Tracker	12
2.3.2 The Calorimeter	12
2.3.3 Anti-Coincidence Detector	12
2.3.4 Gamma-ray Burst Monitor	12
2.4 Astrophysical Sources of Gamma-rays	12
2.4.1 Pulsars	12
2.4.2 Pulsar Wind Nebulae	14
2.5 Radiation Processes in Gamma-ray Astrophysics	17
2.5.1 Synchrotron	18
2.5.2 Inverse Compton	19
2.5.3 Bremsstrahlung	20
2.5.4 Pion Decay	21
2.6 The Galactic Diffuse and Isotropic Gamma-ray Background	21
2.7 Sources Detected by the Fermi the Large Area Telescope	22

2.7.1	The Second Fermi Catalog	22
2.7.2	The Second Fermi Pulsar Catalog	23
2.7.3	Pulsar Wind Nebulae Detected by The Large Area Telescope .	23
3	The Pulsar/Pulsar Wind Nebula System	25
3.1	Neutron Star Formation	25
3.2	Pulsar Evolution	26
3.3	Pulsar Magnetosphere	30
3.4	Pulsar Wind Nebulae Structure	31
3.5	Pulsar Wind Nebula Emission	35
4	Maximum-likelihood analysis of LAT data	37
4.1	Motivations for Maximum-Likelihood Analysis of Gamma-ray Data .	38
4.2	Description of Maximum-Likelihood Analysis	39
4.3	Defining a Model of the Sources in the Sky	39
4.4	The LAT Instrument Response Functions	42
4.5	Binned Maximum-Likelihood of LAT Data with the Science Tools . .	44
4.6	The Alternate Maximum-Likelihood Package <code>pointlike</code>	46
5	Analysis of Spatially Extended LAT Sources	47
5.1	Introduction	47
5.2	Analysis Method	50
5.2.1	Modeling Extended Sources in the <code>pointlike</code> Package	50
5.2.2	Extension Fitting	52
5.2.3	<code>gtlike</code> Analysis Validation	55
5.2.4	Comparing Source Sizes	55
5.3	Validation of the TS Distribution	57
5.3.1	Point-like Source Simulations Over a Uniform Background . .	57
5.3.2	Point-like Source Simulations Over a Structured Background .	59
5.3.3	Extended Source Simulations Over a Structured Background .	63
5.4	Extended Source Detection Threshold	68
5.5	Testing Against Source Confusion	70

5.6	Test of 2LAC Sources	79
6	Search for Spatially-extended LAT Sources	83
6.1	Analysis of Extended Sources Identified in the 2FGL Catalog	84
6.2	Systematic Errors on Extension	85
6.3	Extended Source Search Method	88
6.4	New Extended Sources	94
6.4.1	2FGL J0823.0–4246	97
6.4.2	2FGL J0851.7–4635	99
6.4.3	2FGL J1615.0–5051	99
6.4.4	2FGL J1615.2–5138	103
6.4.5	2FGL J1627.0–2425c	104
6.4.6	2FGL J1632.4–4753c	105
6.4.7	2FGL J1712.4–3941	108
6.4.8	2FGL J1837.3–0700c	110
6.4.9	2FGL J2021.5+4026	112
6.5	Discussion	115
7	Search for PWNe associated with Gamma-loud Pulsars	121
7.1	Off-peak Phase Selection	121
7.2	Off-peak Analysis Method	121
7.3	Off-peak Results	121
7.4	Off-Peak Individual Source Discussion	121
8	Search for PWNe associated with TeV Pulsars	122
8.1	Introduction	123
8.2	List of very high energy (VHE) PWN Candidates	123
8.3	Analysis Method	126
8.4	Sources Detected	128
9	Population Study of LATs-detected PWNe	131
9.1	Summary of the PWNe detected by the LATs	132

9.2	The Evolution of γ -ray Emitting PWNe with the Properties of their Pulsars	132
10	Future Work (or Outlook)??	137

List of Tables

5.1	Monte Carlo Spectral Parameters	62
5.2	Extension Detection Threshold	71
6.1	Analysis of the twelve extended sources included in the 2FGL catalog	86
6.2	Nearby Residual-induced Sources	93
6.3	Extension fit for the nine additional extended sources	95
6.4	Dual localization, alternative PSF, and alternative approach to modeling the diffuse emission	96
8.1	List of analyzed VHE sources	124
8.1	List of analyzed VHE sources	125
8.2	Spatial and spectral results for detected VHE sources	129
9.1	133
9.1	134

List of Figures

2.1	Transparency of the atmosphere of the earth to photons of varying wavelenthts. This figure is from Carroll & Ostlie (2006)	5
2.2	The experimental design of Explorer XI. This figure is from Kraushaar et al. (1965).	7
2.3	The position of all 621 cosmic γ -rays detected by the Third Orbiting Solar Observatory (OSO-3). This figure is from Kraushaar et al. (1972).	8
2.4	A map of the sources observed by COS-B. The filled circles represent brighter sources. The unshaded region corresponds to the parts of the sky observed by COS-B. This figure is from Swanenburg et al. (1981).	10
2.5	The position of the Energetic Gamma Ray Experiment Telescope (EGRET) sources in the sky in galactic coordinates. The size of the source markers corresponds to the overall source intensity. This figure is from (Hartman et al. 1999).	11
2.6	The Orion plate from Bevis' book <i>Uranographia Britannica</i> . The Crab nebula can be found on the horn of Taurus the Bull on the top of the figure and the source is marked by a cloudy symbol. This figure was reproduced from Ashworth (1981).	15
3.1	The rotating dipole model of a puslar. This figure is taken from (Carroll & Ostlie 2006).	27
3.2	The magnetosphere for a rotating pulsar. The pulsar is on the bottom left of the plot. This figure is from Goldreich & Julian (1969).	30

3.3	The regions of emission in a pulsar/PWN system. This figure shows (top) the pulsar's magnetosphere, (middle), the unshocked pulsar wind and (bottom) the shocked pulsar wind which can be observed as the PWN. "R", "O", "X", and " γ " describe sites of radio, optical, X-ray, and γ -ray emission respectively. "CR", "Sy", and "IC" refer to regions of curvature, inverse Compton, and synchrotron emission. Figure is taken from Aharonian & Bogovalov (2003).	33
5.1	Counts maps and TS profiles for the SNR IC 443. (a) TS vs. extension of the source. (b) TS_{ext} for individual energy bands. (c) observed radial profile of counts in comparison to the expected profiles for a spatially extended source (solid and colored red in the online version) and for a point-like source (dashed and colored blue in the online version). (d) smoothed counts map after subtraction of the diffuse emission compared to the smoothed LAT PSF (inset). Both were smoothed by a 0.1° 2D Gaussian kernel. Plots (a), (c), and (d) use only photons with energies between 1 GeV and 100 GeV. Plots (c) and (d) include only photons which converted in the front part of the tracker and have an improved angular resolution (Atwood et al. 2009).	54
5.2	A comparison of a 2D Gaussian and uniform disk spatial model of extended sources before and after convolving with the PSF for two energy ranges. The solid black line is the PSF that would be observed for a power-law source of spectral index 2. The dashed line and the dash-dotted lines are the brightness profile of a Gaussian with $r_{68} = 0.5$ and the convolution of this profile with the LAT PSF respectively (colored red in the online version). The dash-dot-dotted and the dot-dotted lines are the brightness profile of a uniform disk with $r_{68} = 0.5$ and the convolution of this profile with the LAT PSF respectively (colored blue in the online version).	56

5.3	Cumulative distribution of the TS for the extension test when fitting simulated point-like sources in the 1 GeV to 100 GeV energy range. The four plots represent simulated sources of different spectral indices and the different lines (colored in the online version) represent point-like sources with different 100 MeV to 100 GeV integral fluxes. The dashed line (colored red) is the cumulative density function of Equation 5.11.	60
5.4	The same plot as Figure 5.3 but fitting in the 10 GeV to 100 GeV energy range.	61
5.5	Cumulative distribution of TS_{ext} for sources simulated on top of the Galactic diffuse and isotropic background.	64
5.6	The distribution of TS values when fitting 985 statistically independent simulations of W44. (a) is the distribution of TS values when fitting W44 as a point-like source and (b) is the distribution of TS_{ext} when fitting the source with a uniform disk or a radially-symmetric Gaussian spatial model. (c) is the distribution of the change in TS when fitting the source with an elliptical disk spatial model compared to fitting it with a radially-symmetric disk spatial model and (d) when fitting the source with an elliptical ring spatial model compared to an elliptical disk spatial model.	66
5.7	The distribution of fit parameters for the Monte Carlo simulations of W44. The plots show the distribution of best fit (a) flux (b) spectral index and (c) 68% containment radius. The dashed vertical lines represent the simulated values of the parameters.	67

5.8	The detection threshold to resolve an extended source with a uniform disk model for a two-year exposure. All sources have an assumed power-law spectrum and the different line styles (colors in the electronic version) correspond to different simulated spectral indices. The lines with no markers correspond to the detection threshold using photons with energies between 100 MeV and 100 GeV, while the lines with star-shaped markers correspond to the threshold using photons with energies between 1 GeV and 100 GeV.	69
5.9	The LAT detection threshold for four spectral indices and three backgrounds ($1\times$, $10\times$, and $100\times$ the Sreekumar-like isotropic background) for a two-year exposure. The left-hand plots are the detection threshold when using photons with energies between 1 GeV and 100 GeV and the right-hand plots are the detection threshold when using photons with energies between 10 GeV and 100 GeV. The flux is integrated only in the selected energy range. Overlaid on this plot are the LAT-detected extended sources placed by the magnitude of the nearby Galactic diffuse emission and the energy range they were analyzed with. The star-shaped markers (colored red in the electronic version) are sources with a spectral index closer to 1.5, the triangular markers (colored blue) an index closer to 2, and the circular markers (colored green) an index closer to 2.5. The triangular marker in plot (d) below the sensitivity line is MSH 15–52.	72

5.10	The projected detection threshold of the LAT to extension after 10 years for a power-law source of spectral index 2 against 10 times the isotropic background in the energy range from 1 GeV to 100 GeV (solid line colored red in the electronic version) and 10 GeV to 100 GeV (dashed line colored blue). The shaded gray regions represent the detection threshold assuming the sensitivity improves from 2 to 10 years by the square root of the exposure (top edge) and linearly with exposure (bottom edge). The lower plot shows the factor increase in sensitivity. For small extended sources, the detection threshold of the LAT to the extension of a source will improve by a factor larger than the square root of the exposure.	73
5.11	(a) and (b) are the distribution of TS_{ext} and of $TS_{2\text{pts}}$ when fitting simulated spatially extended sources of varying sizes as both an extended source and as two point-like sources. (c) and (d) are the distribution of $TS_{\text{ext}} - TS_{2\text{pts}}$ for the same simulated sources. (a) and (c) represent sources fit in the 1 GeV to 100 GeV energy range and (b) and (d) represent sources fit in the 10 GeV to 100 GeV energy range. In (c) and (d), the plus-shaped markers (colored red in the electronic version) are fits where $TS_{\text{ext}} \geq 16$	76
5.12	The distribution of $TS_{\text{ext}} - TS_{2\text{pts}}$ when fitting two simulated point-like sources of varying separations as both an extended source and as two point-like sources. (a), and (b) represent simulations of two point-like sources with the same spectral index and (c) and (d) represent simulations of two point-like sources with different spectral indices. (a) and (c) fit the simulated sources in the 1 GeV to 100 GeV energy range and (b) and (d) fit in the 10 GeV to 100 GeV energy range. The plus-shaped markers (colored red in the electronic version) are fits where $TS_{\text{ext}} \geq 16$	77

5.13	The cumulative density of TS_{ext} for the 733 clean AGN in 2LAC that were significant above 1 GeV calculated with <code>pointlike</code> (dashed line colored blue in the electronic version) and with <code>gtlike</code> (solid line colored black). AGN are too far and too small to be resolved by the LAT. Therefore, the cumulative density of TS_{ext} is expected to follow a $\chi^2_1/2$ distribution (Equation 5.11, the dash-dotted line colored red).	81
6.1	A TS map generated for the region around the SNR IC 443 using photons with energies between 1 GeV and 100 GeV. (a) TS map after subtracting IC 443 modeled as a point-like source. (b) same as (a), but IC 443 modeled as an extended source. The cross represents the best fit position of IC 443.	90
6.2	A diffuse-emission-subtracted 1 GeV to 100 GeV counts map of the region around 2FGL J1856.2+0450c smoothed by a $0^\circ.1$ 2D Gaussian kernel. The plus-shaped marker and circle (colored red in the online version) represent the center and size of the source fit with a radially-symmetric uniform disk spatial model. The black crosses represent the positions of other 2FGL sources. The extension is statistically significant, but the extension encompasses many 2FGL sources and the emission does not look to be uniform. Although the fit is statistically significant, it likely corresponds to residual features of inaccurately modeled diffuse emission picked up by the fit.	92

- 6.3 A diffuse-emission-subtracted 1 GeV to 100 GeV counts map of 2FGL J0823.0–4246 smoothed by a $0^\circ.1$ 2D Gaussian kernel. The triangular marker (colored red in the online version) represents the 2FGL position of this source. The plus-shaped marker and the circle (colored red) represent the best fit position and extension of this source assuming a radially-symmetric uniform disk model. The two star-shaped markers (colored green) represent 2FGL sources that were removed from the background model. From left to right, these sources are 2FGL J0823.4–4305 and 2FGL J0821.0–4254. The lower right inset is the model predicted emission from a point-like source with the same spectrum as 2FGL J0823.4–4305 smoothed by the same kernel. This source is spatially coincident with the Puppis A SNR. The light blue contours correspond to the X-ray image of Puppis A observed by *ROSAT* (Petre et al. 1996). 98
- 6.4 A diffuse-emission-subtracted 10 GeV to 100 GeV counts map of 2FGL J0851.7–4635 smoothed by a $0^\circ.25$ 2D Gaussian kernel. The triangular marker (colored red in the electronic version) represents the 2FGL position of this source. The plus-shaped marker and the circle (colored red) are the best fit position and extension of this source assuming a radially-symmetric uniform disk model. The three black crosses represent background 2FGL sources. The three star-shaped markers (colored green) represent other 2FGL sources that were removed from the background model. They are (from left to right) 2FGL J0853.5–4711, 2FGL J0855.4–4625, and 2FGL J0848.5–4535. The circular and square-shaped marker (colored blue) represents the 2FGL and relocalized position of another 2FGL source. This extended source is spatially coincident with the Vela Jr. SNR. The contours (colored light blue) correspond to the TeV image of Vela Jr. (Aharonian et al. 2007b). . . 100

- 6.5 A diffuse-emission-subtracted 10 GeV to 100 GeV counts map of 2FGL J1615.0–5051 (upper left) and 2FGL J1615.2–5138 (lower right) smoothed by a $0^\circ.1$ 2D Gaussian kernel. The triangular markers (colored red in the electronic version) represent the 2FGL positions of these sources. The cross-shaped markers and the circles (colored red) represent the best fit positions and extensions of these sources assuming a radially symmetric uniform disk model. The two black crosses represent background 2FGL sources and the star-shaped marker (colored green) represents 2FGL J1614.9-5212, another 2FGL source that was removed from the background model. The contours (colored light blue) correspond to the TeV image of HESS J1616–508 (left) and HESS J1614–518 (right) (Aharonian et al. 2006e). 101
- 6.6 A diffuse-emission-subtracted 1 GeV to 100 GeV counts map of (a) the region around 2FGL J1627.0–2425 smoothed by a $0^\circ.1$ 2D Gaussian kernel and (b) with the emission from 2FGL J1625.7–2526 subtracted. The triangular marker (colored red in the online version) represents the 2FGL position of this source. The plus-shaped marker and the circle (colored red) represent the best fit position and extension of this source assuming a radially-symmetric uniform disk model and the black cross represents a background 2FGL source. The contours in (a) correspond to the $100\ \mu\text{m}$ image observed by IRAS (Young et al. 1986). The contours in (b) correspond to CO ($J = 1 \rightarrow 0$) emission integrated from $-8\ \text{km s}^{-1}$ to $20\ \text{km s}^{-1}$. They are from de Geus et al. (1990), were cleaned using the moment-masking technique (Dame 2011), and have been smoothed by a $0^\circ.25$ 2D Gaussian kernel. 104

- 6.7 A diffuse-emission-subtracted 10 GeV to 100 GeV counts map of 2FGL J1632.4–4753c (a) smoothed by a 0.1° 2D Gaussian kernel and (b) with the emission from the background sources subtracted. The triangular marker (colored red in the electronic version) represents the 2FGL position of this source. The plus-shaped marker and the circle (colored red) are the best fit position and extension of 2FGL J1632.4–4753c assuming a radially-symmetric uniform disk model. The four black crosses represent background 2FGL sources subtracted in (b). The circular and square-shaped markers (colored blue) represent the 2FGL and relocalized positions respectively of two additional background 2FGL sources subtracted in (b). The star-shaped marker (colored green) represents 2FGL J1634.4–4743c, another 2FGL source that was removed from the background model. The contours (colored light blue) correspond to the TeV image of HESS J1632–478 (Aharonian et al. 2006e). . . . 106
- 6.8 The spectral energy distribution of four extended sources associated with unidentified extended TeV sources. The black points with circular markers are obtained by the LAT. The points with plus-shaped markers (colored red in the electronic version) are for the associated H.E.S.S. sources. (a) the LAT SED of 2FGL J1615.0–5051 together with the H.E.S.S. SED of HESS J1616–508. (b) 2FGL J1615.2–5138 and HESS J1614–518. (c) 2FGL J1632.4–4753c and HESS J1632–478. (d) 2FGL J1837.3–0700c and HESS J1837–069. The H.E.S.S. data points are from (Aharonian et al. 2006e). Both LAT and H.E.S.S. spectral errors are statistical only. 107

6.9	A diffuse-emission-subtracted 10 GeV to 100 GeV counts map of 2FGL J1712.4–3941 (a) smoothed by a $0^\circ.15$ 2D Gaussian kernel and (b) with the emission from the background sources subtracted. This source is spatially coincident with RX J1713.7–3946 and was recently studied in Abdo et al. (2011). The triangular marker (colored red in the online version) represents the 2FGL position of this source. The plus-shaped marker and the circle (colored red) are the best fit position and extension of this source assuming a radially symmetric uniform disk model. The two black crosses represent background 2FGL sources subtracted in (b). The contours (colored light blue) correspond to the TeV image (Aharonian et al. 2007c).	109
6.10	A diffuse-emission-subtracted 10 GeV to 100 GeV counts map of the region around 2FGL J1837.3–0700c (a) smoothed by a $0^\circ.15$ 2D Gaussian kernel and (b) with the emission from the background sources subtracted. The triangular marker (colored red in the online version) represents the 2FGL position of this source. The plus-shaped marker and the circle (colored red) represent the best fit position and extension of 2FGL J1837.3–0700c assuming a radially-symmetric uniform disk model. The circular and square-shaped markers (colored blue) represent the 2FGL and the relocalized positions respectively of two background 2FGL sources subtracted in (b). The star-shaped marker (colored green) represents 2FGL J1835.5–0649, another 2FGL source that was removed from the background model. The contours (colored light blue) correspond to the TeV image of HESS J1837–069 (Aharonian et al. 2006e). The diamond-shaped marker (colored orange) represents the position of PSR J1838–0655 and the hexagonal-shaped marker (colored purple) represents the position AX J1837.3–0652 (Gotthelf & Halpern 2008).	111

- 6.11 A diffuse-emission-subtracted 10 GeV to 100 GeV counts map of the region around 2FGL J2021.5+4026 smoothed by a 0.1° 2D Gaussian kernel. The triangular marker (colored red in the online version) represents the 2FGL position of this source. The plus-shaped marker and the circle (colored red) represent the best fit position and extension of 2FGL J2021.5+4026 assuming a radially-symmetric uniform disk model. The star-shaped marker (colored green) represents 2FGL J2019.1+4040, a 2FGL source that was removed from the background model. 2FGL J2021.5+4026 is spatially coincident with the γ -Cygni SNR. The contours (colored light blue) correspond to the 408MHz image of γ -Cygni observed by the Canadian Galactic Plane Survey (Taylor et al. 2003). 113
- 6.12 The spectral energy distribution of the extended sources Puppis A (2FGL J0823.0–4246) and γ -Cygni (2FGL J2021.5+4026). The lines (colored red in the online version) are the best fit power-law spectral models of these sources. Puppis A has a spectral index of 2.21 ± 0.09 and γ -Cygni has an index of 2.42 ± 0.19 . The spectral errors are statistical only. The upper limit is at the 95% confidence level. . . . 114
- 6.13 The 21 spatially extended sources detected by the LAT at GeV energies with 2 years of data. The twelve extended sources included in 2FGL are represented by the circular markers (colored red in the online version). The nine new extended sources are represented by the triangular markers (colored orange). The source positions are overlaid on a 100 MeV to 100 GeV Aitoff projection sky map of the LAT data in Galactic coordinates. 116

6.14	A comparison of the sizes of extended sources detected at both GeV and TeV energies. The TeV sizes of W30, 2FGL J1837.3–0700c, 2FGL J1632.4–4753c, 2FGL J1615.0–5051, and 2FGL J1615.2–5138 are from Aharonian et al. (2006e). The TeV sizes of MSH 15–52, HESS J1825–137, Vela X, Vela Jr., RX J1713.7–3946 and W28 are from Aharonian et al. (2005a, 2006c,d, 2007b,c, 2008a). The TeV size of IC 443 is from Acciari et al. (2009) and W51C is from Krause et al. (2011). The TeV sizes of MSH 15–52, HESS J1614–518, HESS J1632–478, and HESS J1837–069 have only been reported with an elliptical 2D Gaussian fit and so the plotted sizes are the geometric mean of the semi-major and semi-minor axis. The LAT extension of Vela X is from Abdo et al. (2010). The TeV sources were fit assuming a 2D Gaussian surface brightness profile so the plotted GeV and TeV extensions were first converted to r_{68} (see Section 5.2.4). Because of their large sizes, the shape of RX J1713.7–3946 and Vela Jr. were not directly fit at TeV energies and so are not included in this comparison. On the other hand, dedicated publications by the LAT collaboration on these sources showed that their morphologies are consistent (Abdo et al. 2011; Tanaka et al. 2011). The LAT extension errors are the statistical and systematic errors added in quadrature.	117
6.15	The distributions of the sizes of 18 extended LAT sources at GeV energies (colored blue in the electronic version) and the sizes of the 40 extended H.E.S.S. sources at TeV energies (colored red). The H.E.S.S. sources were fit with a 2D Gaussian surface brightness profile so the LAT and H.E.S.S. sizes were first converted to r_{68} . The GeV size of Vela X is taken from Abdo et al. (2010). Because of their large sizes, the shape of RX J1713.7–3946 and Vela Jr. were not directly fit at TeV energies and are not included in this comparison. Centaurus A is not included because of its large size.	118

6.16	The distribution of spectral indices of the 1873 2FGL sources (colored red in the electronic version) and the 21 spatially extended sources (colored blue). The index of Centaurus A is taken from Nolan et al. (2012) and the index of Vela X is taken from Abdo et al. (2010).	120
9.1	...	134
9.2	...	135
9.3	...	136

List of Acronyms

- 1FHL** the first *Fermi* hard-source list. 126
- 2CG** the second COS-B catalog. 9
- 2FGL** the second *Fermi* catalog. 22, 38, 122, 127
- 2PC** the second *Fermi* pulsar catalog. 23, 124, 125
- 3EG** the Third EGRET Catalog. 11
- ACD** Anti-Coincidence Detector. vii, 12
- arcsec** second of arc. 32
- BPL** broken-power law. 40
- CGRO** the Compton Gamma Ray Observatory. 10
- CGS** the Centimetre-Gram-Second System of Units. 40, 41
- ECPL** exponentially-cutoff power law. 40, 41
- EGRET** the Energetic Gamma Ray Experiment Telescope. xii, 9–11
- ESA** the European Space Agency. 9
- FWHM** full width at half maximum. 8
- GBM** Gamma-ray Burst Monitor. vii, 12

IACT Imaging air Cherenkov detector. 48, 119, 122, 126

IC inverse Compton. 6, 19, 20, 31, 32, 35, 126

LAT the Large Area Telescope. iv, v, vii, viii, 12, 22, 23, 122, 123, 125–127, 129, 131

MIT the Massachusetts Institute of Technology. 6, 13

MSC massive star cluster. 125

MSP millisecond pulsar. 27

NASA the National Aeronautics and Space Administration. 9, 10

NRL the Naval Research Laboratory. 13

NS neutron star. 13, 25, 26, 30

OSO-3 the Third Orbiting Solar Observatory. xii, 8, 9, 22

PL power law. 40, 41

PSF point spread function. 126

PWN pulsar wind nebula. iv, v, xiii, 1, 6, 14, 25, 29, 31–35, 122, 123, 125–129, 131

SA solid angle. 42, 43

SAS-2 the second Small Astronomy Satellite. 9, 10

SNR supernova remnant. 29, 32, 41

UNID unidentified source. 125, 126

VHE very high energy. ix, xi, 122–129, 133

Chapter 9

Population Study of LATs-detected PWNe

This chapter is based the second part of the the paper “Constraints on the Galactic Population of TeV Pulsar Wind Nebulae using Fermi Large Area Telescope Observations” by Acero et al which is currently in prep.

In Chapter 6, we search for new spatially-extended *Fermi* sources and found that spatial extension was an important characteristic for detecting new pulsar wind nebulae (PWNe). In the process, we discovered three new γ -ray emitting PWNs. In Chapter 7, we then searched in the off-peak phase interval of the Large Area Telescope (LAT)-detected pulsars for new pulsar wind nebula and discovered 3C 58. Finally, in Chapter 8 we searched in the regions surrounding PWNs candidates detected at TeV energies for GeV-emitting PWNs 4 new PWNe candidates (HESS J1119–614, HESS J1303–631, HESS J1420–607, and HESS J1841–055) and 1 new PWN (HESS J1356–645)

In this chapter, we take the population of γ -ray emitting PWNs and PWNs candidates

9.1 Summary of the PWNe detected by the LATs

9.2 The Evolution of γ -ray Emitting PWNe with the Properties of their Pulsars

Table 9.1.

Source	\dot{E} (erg s ⁻¹)	τ (kyr)	Distance (kpc)	Flux TeV	Flux Xray
VERJ0006+727	4.5e+35	13.9	1.4 +0.3 -0.3
Crab	4.6e+38	1.2	2.0 +0.5 -0.5	80.0 +/- 16.49242	21000.0 +/- 4200.0
MGROJ0631+105	1.7e+35	43.6	1.0 +0.2 -0.2
MGROJ0632+17	3.2e+34	342	0.2 +0.01 -0.02
Vela-X	6.9e+36	11.3	0.3 +0.02 -0.02	79.0 +/- 21.2132	53.9 +/- 17.8
HESSJ1018-589	2.6e+36	21	2.9 +1.6 -0.06	0.9 +/- 0.4	...
HESSJ1023-577	1.1e+37	4.6	2.8 +0.0 -0.0	4.82411 +/- 1.70053	...
HESSJ1026-582	8.4e+35	90	2.3 +0.3 -0.3	3.73537 +/- 2.18879	...
HESSJ1119-614	2.3e+36	1.6	8.4 +0.4 -0.4	2.3188 +/- 1.15666	...
HESSJ1303-631	1.7e+36	11	6.65 +1.2 -1.1	26.7 +/- 1.0	0.16 +/- 0.03
HESSJ1356-645	3.1e+36	7.3	2.5 +0.53 -0.44	6.66231 +/- 3.71138	0.0604 +/- 0.012
HESSJ1418-609	4.9e+36	1.03	1.6 +0.7 -0.7	3.41 +/- 1.82	3.11 +/- 0.147
HESSJ1420-607	1.0e+37	13	5.6 +0.91 -0.85	14.5 +/- 3.3	1.3 +/- 0.26
HESSJ1458-608	9.1e+35	64.7	4.0 +0.0 -0.0	2.45224 +/- 0.68099	...
HESSJ1514-591	1.7e+37	1.56	4.2 +0.6 -0.6	20.3 +/- 4.25	28.6 +/- 5.72
HESSJ1554-550	...	18	7.5 +1.3 -1.3	...	3.07 +/- 1.0
HESSJ1616-508	1.6e+37	8.13	6.8 +0.7 -0.7	21.0 +/- 5.0	4.2 +/- 0.84
HESSJ1632-478	3.0e+36	20	3.0 +0.0 -0.0	14.8003 +/- 4.71778	0.43 +/- 0.08
HESSJ1640-465	4.0e+36	...	8.6 +0.0 -0.0	5.46577 +/- 1.23707	0.46 +/- 0.092
HESSJ1646-458B	2.1e+35	110	5.7 +0.7 -0.7	3.0 +/- 0.8	...
HESSJ1702-420	3.4e+35	55	4.8 +0.6 -0.5	9.1 +/- 3.4	0.006 +/- 0.0
HESSJ1708-443	3.4e+36	17.5	2.3 +0.3 -0.3	22.88 +/- 6.96	0.72 +/- 0.0339
HESSJ1718-385	1.3e+36	89.5	4.24 +0.4 -0.4	4.3 +/- 1.6	0.14 +/- 0.028
HESSJ1804-216	2.2e+36	16	3.8 +0.5 -0.4	11.8 +/- 2.4	0.068 +/- 0.0136
HESSJ1809-193	1.8e+36	51.3	3.5 +0.4 -0.4	19.0 +/- 5.66	0.23 +/- 0.046
HESSJ1813-178	6.8e+37	5.4	...	4.97349 +/- 0.6491	...
HESSJ1818-154	2.3e+33	9	7.8 +1.4 -1.6	1.29742 +/- 0.90339	...
HESSJ1825-137	2.8e+36	21	4.12 +0.4 -0.4	61.0 +/- 13.89	0.44 +/- 0.088
HESSJ1831-098	1.1e+36	128	4.0 +0.4 -0.4	5.08 +/- 0.58	...
HESSJ1833-105	3.4e+37	4.85	4.7 +0.4 -0.5	2.4 +/- 1.21	40.0 +/- 0.0
HESSJ1837-069	5.5e+36	2.23	6.6 +0.9 -0.9	22.9 +/- 8.58	0.639 +/- 0.243
HESSJ1841-055	5.9e+36	4.97	1.3 +0.0 -0.0	23.47835 +/- 3.43665	...
HESSJ1846-029	8.97 +/- 1.51	29.4 +/- 1.39
HESSJ1848-018	6.0 +0.0 -0.0	4.32062 +/- 0.9902	...
HESSJ1849-000	9.8e+36	42.9	7.0 +0.0 -0.0	2.12 +/- 0.41	0.9 +/- 0.2
HESSJ1857+026	4.6e+36	20.6	9.0 +1.2 -1.2	18.41 +/- 2.88	...
MGROJ1908+06	2.8e+36	19.5	3.2 +0.3 -0.3	11.9 +/- 4.77	...
HESSJ1912+101	2.9e+36	169	4.8 +0.7 -0.5	7.27 +/- 3.731	...

Table 9.1 (cont'd)

Source	\dot{E} (erg s $^{-1}$)	τ (kyr)	Distance (kpc)	Flux TeV	Flux Xray
VERJ1930+188	1.2e+37	2.89	9.0 +2.0 -7.0	2.26 +/- 1.28	5.23 +/- 0.122
VERJ1959+208	1.6e+35	...	2.5 +1.0 -1.0
MGROJ2019+37	3.4e+36	17.2	8.0 +0.0 -0.0
MGROJ2228+611	2.2e+37	10.5	7.3 +2.2 -3.3	...	0.884 +/- 0.0206

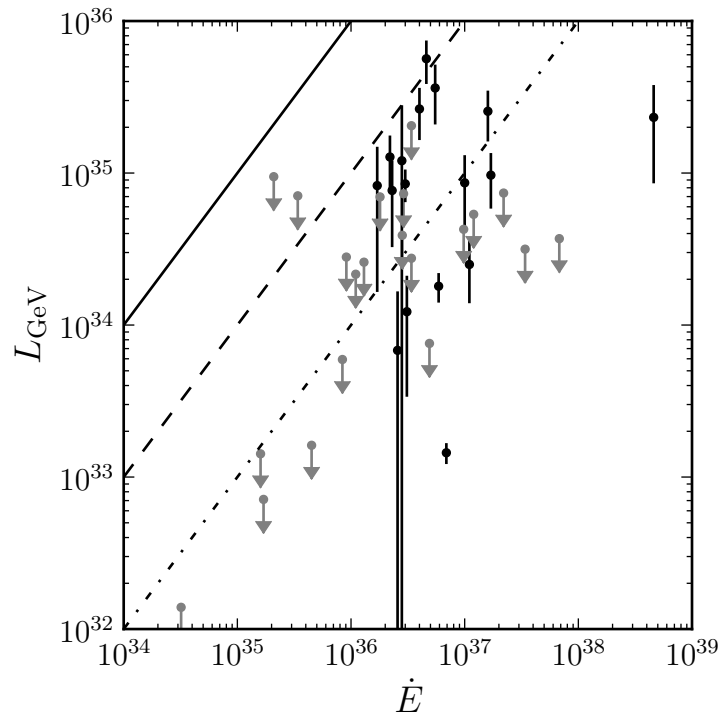


Figure 9.1 ...

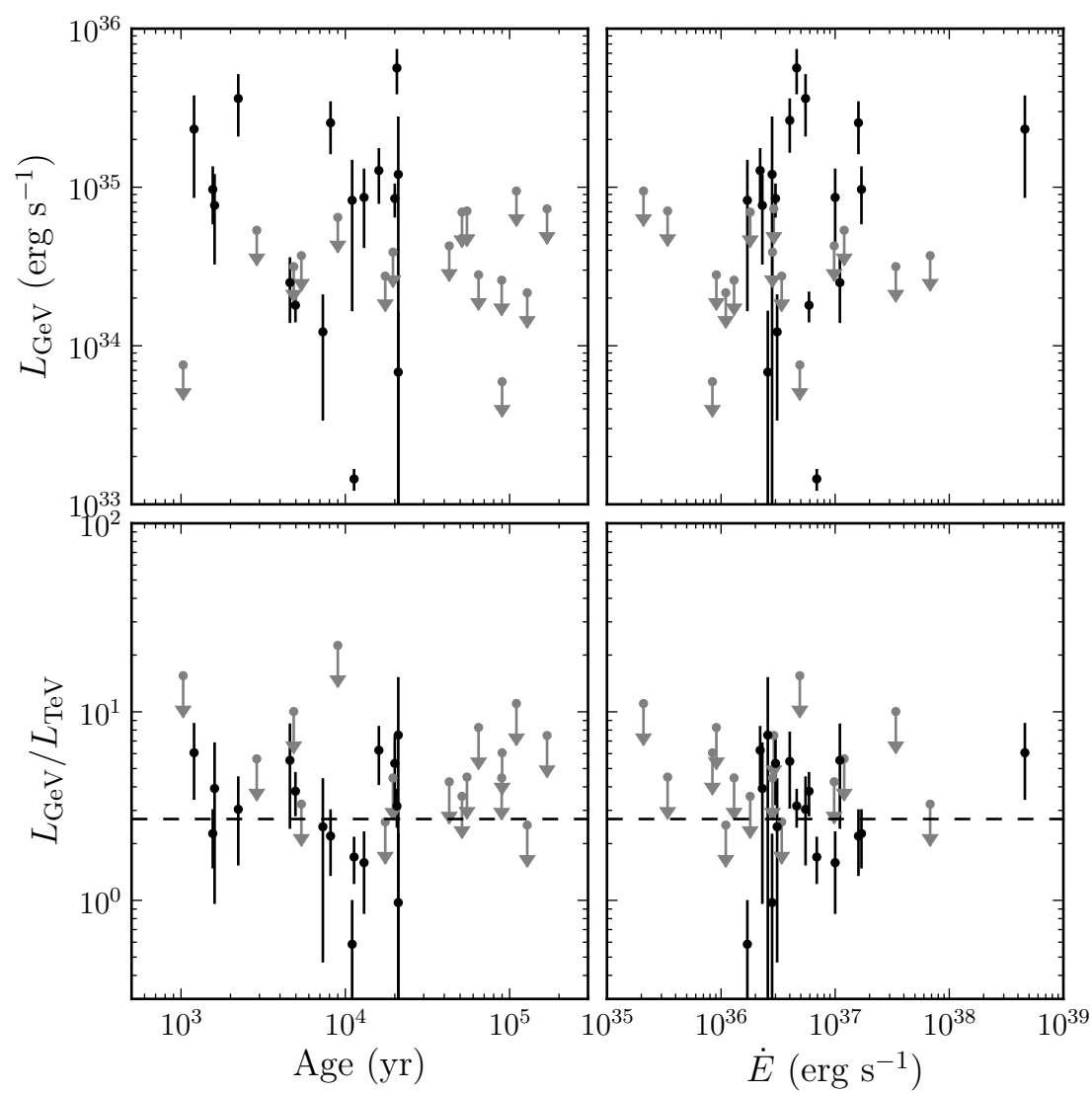


Figure 9.2 ...

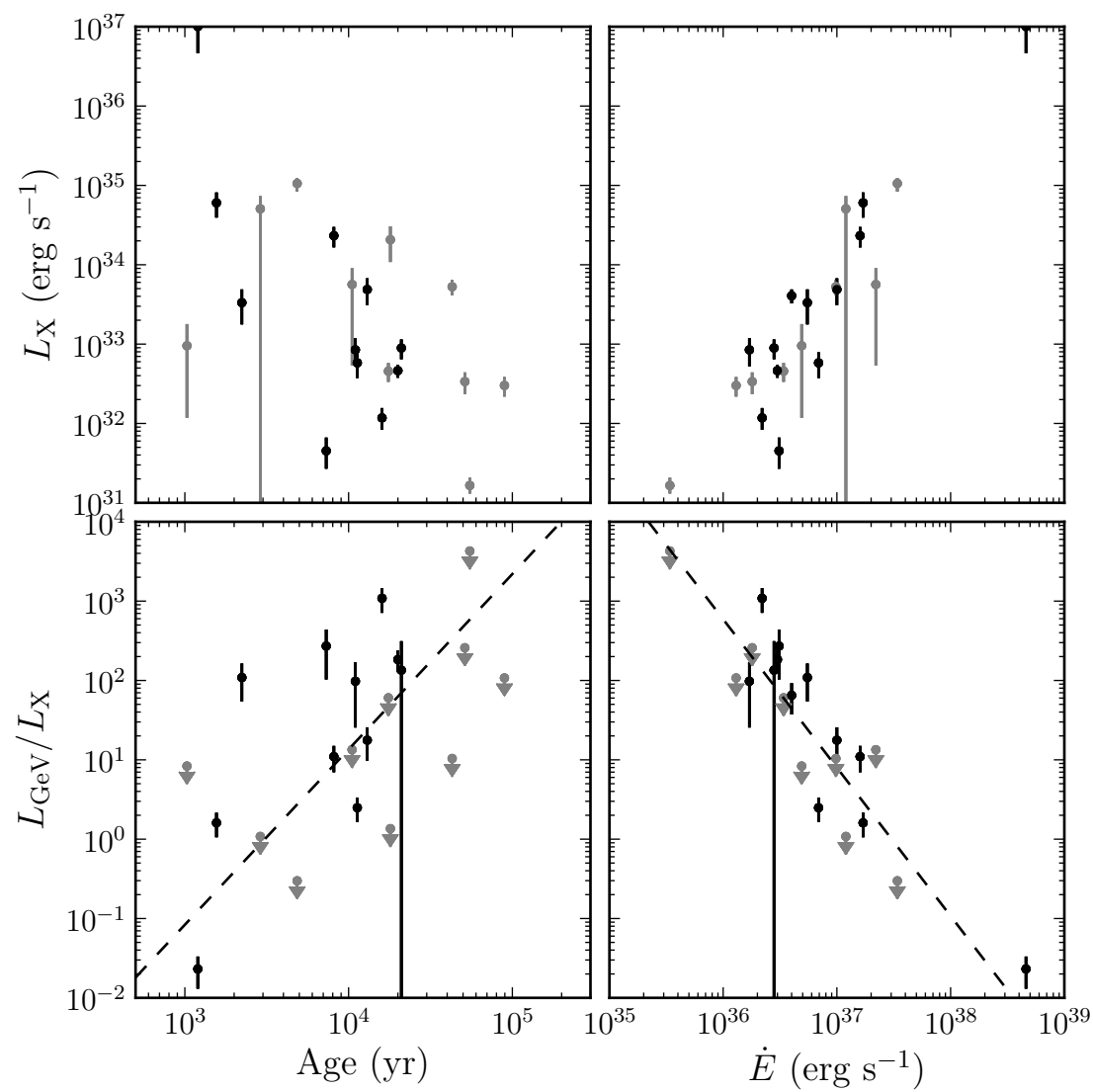


Figure 9.3 ...

Bibliography

- Abdo, A., Ackermann, M., Ajello, M., et al. 2010, *Astrophys.J.*, 722, 1303
- Abdo, A. A., Allen, B., Berley, D., et al. 2007, *ApJ*, 664, L91
- Abdo, A. A., Ackermann, M., Ajello, M., et al. 2009a, *ApJ*, 706, L1
- . 2009b, *ApJS*, 183, 46
- Abdo, A. A., Allen, B. T., Aune, T., et al. 2009c, *ApJ*, 700, L127
- Abdo, A. A., Ackermann, M., Ajello, M., et al. 2009d, *Astroparticle Physics*, 32, 193
- . 2010a, *ApJ*, 714, 927
- Abdo, A. A., Ackermann, M., Ajello, M., et al. 2010b, *A&A*, 523, A46
- Abdo, A. A., Ackermann, M., Ajello, M., et al. 2010c, *Science*, 328, 725
- . 2010d, *ApJS*, 188, 405
- . 2010e, *ApJ*, 708, 1254
- . 2010f, *ApJ*, 718, 348
- Abdo, A. A., Ackermann, M., Ajello, M., et al. 2010, *The Astrophysical Journal*, 713, 146
- Abdo, A. A., Ackermann, M., Ajello, M., et al. 2010a, *Science*, 327, 1103
- . 2010b, *ApJ*, 712, 459

- Abdo, A. A., Ackermann, M., Ajello, M., et al. 2010c, *A&A*, 512, A7
- Abdo, A. A., Ackermann, M., Ajello, M., et al. 2010d, *Physical Review Letters*, 104, 101101
- . 2010e, *ApJS*, 187, 460
- . 2011, *ApJ*, 734, 28
- Acciari, V. A., Aliu, E., Arlen, T., et al. 2009, *ApJ*, 698, L133
- . 2010, *ApJ*, 719, L69
- . 2011, *ApJ*, 738, 3
- Acerro, F., Ackermann, M., Ajello, M., & et al. in prep., *ApJ*
- Acerro, F., Djannati-Ataï, A., Förster, A., et al. 2012, *ArXiv e-prints*
- Ackermann, M., Ajello, M., Allafort, A., et al. in prep, *ApJ*
- . 2011, *ApJ*, 743, 171
- Ackermann, M., Ajello, M., Albert, A., et al. 2012, *ApJS*, 203, 4
- Aharonian, F., Akhperjanian, A. G., Aye, K.-M., et al. 2005a, *A&A*, 435, L17
- . 2005b, *A&A*, 439, 1013
- Aharonian, F., Akhperjanian, A. G., Bazer-Bachi, A. R., et al. 2006a, *A&A*, 460, 743
- . 2006b, *A&A*, 456, 245
- . 2006c, *A&A*, 460, 365
- . 2006d, *A&A*, 448, L43
- . 2006e, *ApJ*, 636, 777
- . 2007a, *A&A*, 472, 489

—. 2007b, *ApJ*, 661, 236

—. 2007c, *A&A*, 464, 235

—. 2008a, *A&A*, 481, 401

Aharonian, F., Akhperjanian, A. G., Barres de Almeida, U., et al. 2008b, *A&A*, 484, 435

—. 2008c, *A&A*, 477, 353

Aharonian, F., Akhperjanian, A. G., Anton, G., et al. 2009, *A&A*, 499, 723

Aharonian, F. A., & Bogovalov, S. V. 2003, *New A*, 8, 85

Aharonian, F. A., Coppi, P. S., & Voelk, H. J. 1994, *ApJ*, 423, L5

Aharonian, F. A., Akhperjanian, A. G., Bazer-Bachi, A. R., et al. 2007d, *A&A*, 469, L1

Ajello, M., Allafort, A., Baldini, L., et al. 2012, *ApJ*, 744, 80

Akaike, H. 1974, *IEEE Transactions on Automatic Control*, 19, 716

Albert, J., Aliu, E., Anderhub, H., et al. 2006, *Science*, 312, 1771

Aliu, E. 2011, in *International Cosmic Ray Conference*, Vol. 7, *International Cosmic Ray Conference*, 227

Arnold, J. R., Metzger, A. E., Anderson, E. C., & van Dilla, M. A. 1962, *J. Geophys. Res.*, 67, 4878

Arons, J. 1996, *Space Sci. Rev.*, 75, 235

Ashworth, William B., J. 1981, *Proceedings of the American Philosophical Society*, 125, pp. 52

Atwood, W. B., Abdo, A. A., Ackermann, M., et al. 2009, *ApJ*, 697, 1071

- Balbo, M., Saouter, P., Walter, R., et al. 2010, *A&A*, 520, A111
- Baltz, E. A., Berenji, B., Bertone, G., et al. 2008, *J. Cosmology Astropart. Phys.*, 7, 13
- Bamba, A., Ueno, M., Koyama, K., & Yamauchi, S. 2003, *The Astrophysical Journal*, 589, 253
- Bartoli, B., Bernardini, P., Bi, X. J., et al. 2012, *ApJ*, 745, L22
- Baum, W. A., Johnson, F. S., Oberly, J. J., et al. 1946, *Phys. Rev.*, 70, 781
- Bertsch, D. L., Brazier, K. T. S., Fichtel, C. E., et al. 1992, *Nature*, 357, 306
- Bignami, G. F., Boella, G., Burger, J. J., et al. 1975, *Space Science Instrumentation*, 1, 245
- Blandford, R. D., & Romani, R. W. 1988, *MNRAS*, 234, 57P
- Blumenthal, G. R., & Gould, R. J. 1970, *Rev. Mod. Phys.*, 42, 237
- Bogovalov, S. V., & Aharonian, F. A. 2000, *MNRAS*, 313, 504
- Bradt, H., Rappaport, S., & Mayer, W. 1969, *Nature*, 222, 728
- Browning, R., Ramsden, D., & Wright, P. J. 1971, *Nature Physical Science*, 232, 99
- Burnham, K. P., & Anderson, D. R. 2002, *Model selection and multimodel inference: a practical information-theoretic approach*, 2nd edn. (Springer)
- Burnight, T. 1949, *Phys. Rev*, 76, 19
- Caballero, I., & Wilms, J. 2012, *Mem. Soc. Astron. Italiana*, 83, 230
- Carroll, B. W., & Ostlie, D. A. 2006, *An Introduction to Modern Astrophysics*, 2nd edn. (Benjamin Cummings)
- Cash, W. 1979, *ApJ*, 228, 939

- Castelletti, G., Dubner, G., Golap, K., & Goss, W. M. 2006, *A&A*, 459, 535
- Chandrasekhar, S. 1931, *ApJ*, 74, 81
- Chaves, R. C. G., Renaud, M., Lemoine-Goumard, M., & Goret, P. 2008, in *American Institute of Physics Conference Series*, Vol. 1085, American Institute of Physics Conference Series, ed. F. A. Aharonian, W. Hofmann, & F. Rieger, 372–375
- Chen, A. W., Piano, G., Tavani, M., et al. 2011, *A&A*, 525, A33
- Cocke, W. J., Disney, M. J., & Taylor, D. J. 1969, *Nature*, 221, 525
- Critchfield, C. L., Ney, E. P., & Oleksa, S. 1952, *Physical Review*, 85, 461
- Dame, T. M. 2011, *ArXiv e-prints*
- de Geus, E. J., Bronfman, L., & Thaddeus, P. 1990, *A&A*, 231, 137
- de los Reyes, R., Zajczyk, A., Chaves, R. C. G., & for the H. E. S. S. collaboration. 2012, *ArXiv e-prints*
- de Naurois, M., & H.E.S.S. Collaboration. 2013, *Advances in Space Research*, 51, 258
- Demorest, P. B., Pennucci, T., Ransom, S. M., Roberts, M. S. E., & Hessels, J. W. T. 2010, *Nature*, 467, 1081
- Djannati-Ataï, A., de Jager, O. C., Terrier, R., & et al. 2008, in *International Cosmic Ray Conference*, Vol. 2, International Cosmic Ray Conference, 823–826
- Eadie, W. T., Drijard, D., & James, F. E. 1971, *Statistical methods in experimental physics* (North-Holland Pub. Co.)
- Espinoza, C. M., Lyne, A. G., Kramer, M., Manchester, R. N., & Kaspi, V. M. 2011, *ApJ*, 741, L13
- Esposito, J. A., Bertsch, D. L., Chen, A. W., et al. 1999, *ApJS*, 123, 203
- Falanga, M., Kuiper, L., Poutanen, J., et al. 2005, *A&A*, 444, 15

- Feenberg, E., & Primakoff, H. 1948, *Phys. Rev.*, 73, 449
- Fichtel, C. E., Hartman, R. C., Kniffen, D. A., et al. 1975, *ApJ*, 198, 163
- Fisher, R. A. 1925, *Statistical Methods for Research Workers* (Edinburgh: Oliver and Boyd)
- Fritz, G., Henry, R. C., Meekins, J. F., Chubb, T. A., & Friedman, H. 1969, *Science*, 164, 709
- Funk, S., Hinton, J. A., Pühlhofer, G., et al. 2007, *ApJ*, 662, 517
- Gaensler, B. M., Schulz, N. S., Kaspi, V. M., Pivovarov, M. J., & Becker, W. E. 2003, *ApJ*, 588, 441
- Gaensler, B. M., & Slane, P. O. 2006, *ARA&A*, 44, 17
- Gaisser, T. K., Protheroe, R. J., & Stanev, T. 1998, *ApJ*, 492, 219
- Gelfand, J. D., Slane, P. O., & Zhang, W. 2009, *ApJ*, 703, 2051
- Giordano, F., & Fermi LAT Collaboration. 2011, in *High-Energy Emission from Pulsars and their Systems*, ed. D. F. Torres & N. Rea, 69
- Gold, T. 1968, *Nature*, 218, 731
- Goldreich, P., & Julian, W. H. 1969, *ApJ*, 157, 869
- Górski, K. M., Hivon, E., Banday, A. J., et al. 2005, *ApJ*, 622, 759
- Gotthelf, E. V., & Halpern, J. P. 2008, *ApJ*, 681, 515
- Grenier, I. A., Casandjian, J.-M., & Terrier, R. 2005, *Science*, 307, 1292
- Grondin, M.-H., Funk, S., Lemoine-Goumard, M., et al. 2011, *ApJ*, 738, 42
- Gunn, J. E., & Ostriker, J. P. 1969, *Nature*, 221, 454
- H. E. S. S. Collaboration, Abramowski, A., Acero, F., et al. 2012, *A&A*, 541, A5

- Hall, T. A., Bond, I. H., Bradbury, S. M., et al. 2003, *ApJ*, 583, 853
- Hartman, R. C., Bertsch, D. L., Bloom, S. D., et al. 1999, *ApJS*, 123, 79
- Haug, E. 1975, *Zeitschrift Naturforschung Teil A*, 30, 1099
- Hayakawa, S. 1952, *Progress of Theoretical Physics*, 8, 571
- Herschel, W. 1800, *Philosophical Transactions of the Royal Society of London*, 90, pp. 284
- H.E.S.S. Collaboration, Abramowski, A., Acero, F., et al. 2011a, *A&A*, 531, A81
- . 2011b, *A&A*, 528, A143
- H.E.S.S. Collaboration, Acero, F., Aharonian, F., et al. 2011c, *A&A*, 525, A45
- H.E.S.S. Collaboration, Abramowski, A., Acero, F., et al. 2011d, *A&A*, 533, A103
- . 2011e, *A&A*, 525, A46
- Hewish, A., Bell, S. J., Pilkington, J. D. H., Scott, P. F., & Collins, R. A. 1968, *Nature*, 217, 709
- Hewitt, J., Grondin, M.-H., Lemoine-Goumard, M., et al. 2012
- Hofverberg, P. 2011, in *International Cosmic Ray Conference*, Vol. 7, *International Cosmic Ray Conference*, 247
- Hoppe, S. 2008, in *International Cosmic Ray Conference*, Vol. 2, *International Cosmic Ray Conference*, 579–582
- Houck, J. C., & Allen, G. E. 2006, *ApJS*, 167, 26
- Hulsizer, R. I., & Rossi, B. 1948, *Phys. Rev.*, 73, 1402
- Hutchinson, G. 1952, *Philosophical Magazine Series 7*, 43, 847
- Hwang, U., Petre, R., & Flanagan, K. A. 2008, *ApJ*, 676, 378

- James, F., & Roos, M. 1975, *Computer Physics Communications*, 10, 343
- Jansky, K. 1933, *Proceedings of the Institute of Radio Engineers*, 21, 1387
- Kargaltsev, O., Pavlov, G. G., & Wong, J. A. 2008, ArXiv e-prints
- Kaspi, V. M., & Helfand, D. J. 2002, in *Astronomical Society of the Pacific Conference Series*, Vol. 271, *Neutron Stars in Supernova Remnants*, ed. P. O. Slane & B. M. Gaensler, 3
- Katagiri, H., Tibaldo, L., Ballet, J., et al. 2011, *ApJ*, 741, 44
- Katsuta, J., Uchiyama, Y., Tanaka, T., et al. 2012
- Kennel, C. F., & Coroniti, F. V. 1984, *ApJ*, 283, 710
- Kerr, M. 2010, PhD thesis, University of Washington
- King, I. 1962, *AJ*, 67, 471
- Klein, O., & Nishina, T. 1929, *Zeitschrift fur Physik*, 52, 853
- Kniffen, D. A., & Fichtel, C. E. 1970, *ApJ*, 161, L157
- Krause, J., Carmona, E., Reichardt, I., & for the MAGIC Collaboration. 2011, ArXiv e-prints
- Kraushaar, W., Clark, G. W., Garmire, G., et al. 1965, *ApJ*, 141, 845
- Kraushaar, W. L., Clark, G. W., Garmire, G. P., et al. 1972, *ApJ*, 177, 341
- Landi, R., de Rosa, A., Dean, A. J., et al. 2007a, *MNRAS*, 380, 926
- Landi, R., Masetti, N., Bassani, L., et al. 2007b, *The Astronomer's Telegram*, 1047, 1
- Large, M. I., Vaughan, A. E., & Mills, B. Y. 1968, *Nature*, 220, 340
- Li, T.-P., & Ma, Y.-Q. 1983, *ApJ*, 272, 317

- Longair, M. S. 2011, *High Energy Astrophysics*, 3rd edn. (The Edinburgh Building, Cambridge CB2 8RU, UK: Cambridge University Press)
- Markwardt, C. B., & Ogelman, H. 1995, *Nature*, 375, 40
- Matsumoto, H., Ueno, M., Bamba, A., et al. 2007, *PASJ*, 59, 199
- Matsumoto, H., Uchiyama, H., Sawada, M., et al. 2008, *PASJ*, 60, 163
- Mattox, J. R., Bertsch, D. L., Fichtel, C. E., et al. 1992, *ApJ*, 401, L23
- Mattox, J. R., Bertsch, D. L., Chiang, J., et al. 1996, *ApJ*, 461, 396
- Mayer-Hasselwander, H. A., Kanbach, G., Bennett, K., et al. 1982, *A&A*, 105, 164
- McArthur, S. 2011, *ArXiv e-prints*
- McK Mahille, J., Schild, R., Wendorf, F., & Brenner, R. 2007, *African Skies*, 11, 2
- Mizukami, T., Kubo, H., Yoshida, T., et al. 2011, *ApJ*, 740, 78
- Morrison, P. 1958, *Il Nuovo Cimento*, 7, 858
- Murphy, T., Mauch, T., Green, A., et al. 2007, *MNRAS*, 382, 382
- Neronov, A., Semikoz, D. V., Tinyakov, P. G., & Tkachev, I. I. 2011, *A&A*, 526, A90
- Nolan, P. L., Arzoumanian, Z., Bertsch, D. L., et al. 1993, *ApJ*, 409, 697
- Nolan, P. L., Fierro, J. M., Lin, Y. C., et al. 1996, *A&AS*, 120, C61
- Nolan, P. L., Abdo, A. A., Ackermann, M., et al. 2012, *ApJS*, 199, 31
- Pacini, F. 1967, *Nature*, 216, 567
- . 1968, *Nature*, 219, 145
- Pacini, F., & Salvati, M. 1973, *ApJ*, 186, 249
- Paron, S., Dubner, G., Reynoso, E., & Rubio, M. 2008, *A&A*, 480, 439

- Petre, R., Becker, C. M., & Winkler, P. F. 1996, *The Astrophysical Journal Letters*, 465, L43
- Pollock, A. M. T. 1985, *A&A*, 150, 339
- Protassov, R., van Dyk, D. A., Connors, A., Kashyap, V. L., & Siemiginowska, A. 2002, *ApJ*, 571, 545
- Rea, N., & Esposito, P. 2011, in *High-Energy Emission from Pulsars and their Systems*, ed. D. F. Torres & N. Rea, 247
- Rees, M. J., & Gunn, J. E. 1974, *MNRAS*, 167, 1
- Renaud, M., Goret, P., & Chaves, R. C. G. 2008, in *American Institute of Physics Conference Series*, Vol. 1085, *American Institute of Physics Conference Series*, ed. F. A. Aharonian, W. Hofmann, & F. Rieger, 281–284
- Reynoso, E. M., Dubner, G. M., Goss, W. M., & Arnal, E. M. 1995, *AJ*, 110, 318
- Reynoso, E. M., Green, A. J., Johnston, S., et al. 2003, *MNRAS*, 345, 671
- Richards, D. W., & Comella, J. M. 1969, *Nature*, 222, 551
- Rodriguez, J., Tomsick, J. A., Foschini, L., et al. 2003, *A&A*, 407, L41
- Rousseau, R., Grondin, M.-H., Van Etten, A., et al. 2012, *A&A*, 544, A3
- Rowell, G., Horns, D., Fukui, Y., & Moriguchi, Y. 2008, in *American Institute of Physics Conference Series*, Vol. 1085, *American Institute of Physics Conference Series*, ed. F. A. Aharonian, W. Hofmann, & F. Rieger, 241–244
- Rybicki, G. B., & Lightman, A. P. 1979, *Radiative processes in astrophysics* (New York: John Wiley & Sons Ltd)
- Schwarz, G. 1978, *The Annals of Statistics*, 6, pp. 461
- Sheidaei, F. 2011, in *International Cosmic Ray Conference*, Vol. 7, *International Cosmic Ray Conference*, 243

- Slane, P., Castro, D., Funk, S., et al. 2010, *The Astrophysical Journal*, 720, 266
- Sreekumar, P., Bertsch, D. L., Hartman, R. C., Nolan, P. L., & Thompson, D. J. 1999, *Astroparticle Physics*, 11, 221
- Sreekumar, P., Bertsch, D. L., Dingus, B. L., et al. 1992, *ApJ*, 400, L67
- Sreekumar, P., Bertsch, D. L., Dingus, B. L., et al. 1998, *The Astrophysical Journal*, 494, 523
- Staelin, D. H., & Reifstein, III, E. C. 1968, *Science*, 162, 1481
- Strong, A. W., & Moskalenko, I. V. 1998, *ApJ*, 509, 212
- Sugizaki, M., Mitsuda, K., Kaneda, H., et al. 2001, *ApJS*, 134, 77
- Swanenburg, B. N., Hermsen, W., Bennett, K., et al. 1978, *Nature*, 275, 298
- Swanenburg, B. N., Bennett, K., Bignami, G. F., et al. 1981, *ApJ*, 243, L69
- Tanaka, T., Allafort, A., Ballet, J., et al. 2011, *ApJ*, 740, L51
- Taylor, A. R., Gibson, S. J., Peracaula, M., et al. 2003, *AJ*, 125, 3145
- Terrier, R., Mattana, F., Djannati-Atai, A., et al. 2008, in *American Institute of Physics Conference Series*, Vol. 1085, *American Institute of Physics Conference Series*, ed. F. A. Aharonian, W. Hofmann, & F. Rieger, 312–315
- Thompson, D. J. 2008, *Reports on Progress in Physics*, 71, 116901
- Thompson, D. J., Fichtel, C. E., Hartman, R. C., Kniffen, D. A., & Lamb, R. C. 1977a, *ApJ*, 213, 252
- Thompson, D. J., Fichtel, C. E., Kniffen, D. A., & Ogelman, H. B. 1977b, *ApJ*, 214, L17
- Thompson, D. J., Bertsch, D. L., Fichtel, C. E., et al. 1993, *ApJS*, 86, 629
- Tomsick, J. A., Lingenfelter, R., Walter, R., et al. 2003, *IAU Circ.*, 8076, 1

Torii, K., Kinugasa, K., Toneri, T., et al. 1998, *ApJ*, 494, L207

van der Swaluw, E., & Wu, Y. 2001, *ApJ*, 555, L49

Vladimirov, A. E., Digel, S. W., Jóhannesson, G., et al. 2011, *Computer Physics Communications*, 182, 1156

Weekes, T. C., Cawley, M. F., Fegan, D. J., et al. 1989, *ApJ*, 342, 379

Weinstein, A., & for the VERITAS Collaboration. 2009, *ArXiv e-prints*

Young, E. T., Lada, C. J., & Wilking, B. A. 1986, *ApJ*, 304, L45